

Materials Advances

Accepted Manuscript

This article can be cited before page numbers have been issued, to do this please use: C. Wang, T. Guo, Y. Gong, X. Wang, P. An, J. Zhang, Z. Gao, W. Gao, Y. Zhang and F. Liu, *Mater. Adv.*, 2025, DOI: 10.1039/D4MA01124D.



This is an Accepted Manuscript, which has been through the Royal Society of Chemistry peer review process and has been accepted for publication.

Accepted Manuscripts are published online shortly after acceptance, before technical editing, formatting and proof reading. Using this free service, authors can make their results available to the community, in citable form, before we publish the edited article. We will replace this Accepted Manuscript with the edited and formatted Advance Article as soon as it is available.

You can find more information about Accepted Manuscripts in the [Information for Authors](#).

Please note that technical editing may introduce minor changes to the text and/or graphics, which may alter content. The journal's standard [Terms & Conditions](#) and the [Ethical guidelines](#) still apply. In no event shall the Royal Society of Chemistry be held responsible for any errors or omissions in this Accepted Manuscript or any consequences arising from the use of any information it contains.

ARTICLE

Novel polydopamine/halloysite nanotubes reinforced brushite calcium phosphate cement for bone regeneration with synergistic regulation mechanical/osteogenic capacity

Chenhao Wang,^a Tao Guo,^{*a} Yukang Gong,^b Xintian Wang,^a Puying An,^a Jie Zhang,^{*a} Zheng Gao,^a Wenshan Gao,^b Yuangong Zhang^a and Feng Liu,^{*a}Received 00th January 20xx,
Accepted 00th January 20xx

DOI: 10.1039/x0xx00000x

Bone regeneration remains a clinical challenge with limited bone substitutes. Brushite calcium phosphates cements (**Bru-CPCs**), possessing good bioactivity and biocompatibility, are one of widely studied for bone graft materials. However, their further application in the long-term remodeling of bone were limited by the low compressive strength. Adding additives have been promising strategy to solve the above problem. Herein, halloysite nanotubes (**HNTs**) with its unique rod-like structure and excellent biocompatibility, were chosen as reinforced materials to fabricate bone repair materials. Inspired by the adhesive proteins in mussels, we modified **HNTs** surface with polydopamine (**PDA**) to improve the inorganic-inorganic phase interfacial interactions between **HNTs** and **Bru-CPCs**. **Bru-CPCs**, **Bru-CPCs/1.5%HNTs** and **Bru-CPCs/1.5%HNTs@PDA** were fabricated and the mechanical properties and biological activity of bone repair materials were evaluated in detail. All the results indicated that **Bru-CPCs** incorporated with **1.5 wt% HNTs@PDA** has good compressive strength and osteo-differentiation properties, which will be a prospective biomaterial for bone-tissue repair.

Introduction

Large bone defects repair has always been a major challenge in the field of orthopedics¹⁻³. Autografts, allografts and xenografts are unable to meet the increasing demand for current clinical needs. Biomaterials have been extensive studied as bone graft⁴⁻⁷. Calcium phosphates cements (**CPCs**), with low-temperature self-setting, high biocompatibility, and similar constituents to bone, has been attracted significant interest as implant materials in bone reconstruction surgery⁸⁻¹². Brushite cements (**Bru-CPCs**) possess superior biodegradability and osteoconductive but inferior mechanical strengths, rendering them unsuitable for current clinical applications¹³⁻¹⁶. Hence, it's important to improve the mechanical strengths of **Bru-CPCs** before using as bone repair materials.

To date, an efficiency strategy is adding additives, such as polymers (chitosan, cellulose ethers, collagen, starch, et. al.), metal ions (Fe^{3+} , Zn^{2+} , Mg^{2+} , Si^{2+} , et al.) and nanoclay (montmorillonite (**MMT**), kaolinite (**Kaol**), laponite (**Lap**), halloysite nanotubes (**HNTs**), et al.), to **CPCs**¹⁷⁻²⁵. Several studied demonstrated the favorable effects of nanoclay on mechanical strengths, cellular adhesion and proliferation. Compared to the other nanoclay, **HNTs** have been widely studied as biomaterials for the excellent biocompatible, unique tubular structure, selectively drug loading, high mechanical strength and abundant resources²⁶⁻²⁹. Research has explored the

function of **HNTs** in modulating osteogenesis.³⁰⁻³³ Firstly, silicate ions released from **HNTs** stimulate osteogenic differentiation and increase the expression of **ALP** and **OCN** genes.³¹ Secondly, the nanotube structure of **HNTs** contributes to the stabilization of extracellular proteins, leading to an upregulation of **ALP** activity.³² Thirdly, **HNTs** that accumulate within cells promote osteogenesis by directly engaging in protein interactions and intracellular signaling pathways.³³ Zhao et al developed a hierarchical composite scaffold with deferoxamine delivery system, **DFO@GMs-PDA/PCL-HNTs** (**DGPN**)³². They demonstrated that **DGPN** can promote bone regeneration and accelerate cranial defect healing. Wu et al. prepared **HNTs**-based bone repair materials³⁰. The incorporation of **HNTs** led to an enhanced mechanical performance and upregulated the expression of osteogenic differentiation-related genes. Ji et al. developed a porous scaffold for bone regeneration by freeze-drying a mixture of nano-scale drug-loaded halloysite nanotubes (**HNTs**) and gelatin.³⁴ The scaffold shows a porous structure and excellent biocompatibility. Compared with the gelatin scaffold, **HNTs** can significantly increase the mechanical properties of the composite scaffold by >300% and match natural cancellous bone. Hence, **HNTs** may be a promising additive for improving the mechanical properties of bone repair materials.

However, the above **HNTs**-based bone repair materials were composed inorganic **HNTs** and organic polymers together. Polymer chains can wrap around **HNTs**, which benefits the modification of interfacial interactions between **HNTs** and the polymer, thereby improving the mechanical properties of bone repair materials^{30, 35, 36}. When introducing **HNTs** into **Bru-CPCs**, the interfacial interactions problem between inorganic **HNTs** and inorganic **Bru-CPCs** may

^a School of Basic Medical Sciences, Hebei University, Baoding 071002, Hebei, China.^b Affiliated Hospital of Hebei University, Hebei University, Baoding 071002, Hebei, China.

Supplementary Information available: [details of any supplementary information available should be included here]. See DOI: 10.1039/x0xx00000x



hinder the mechanical properties of **Bru-CPCs**. Polydopamine (**PDA**) can be prepared via the self-polymerization of dopamine (**DA**) in alkaline solution. The strong covalent or noncovalent interactions (hydrogen bonds or stacking interactions, between catechol moieties and substrates) endows the extraordinary adhesive property to **PDA**. Numerous studies demonstrated that **PDA** coating is universal to nearly all substrates, which is like that of mussel adhesive protein, and it endows substrates biocompatibility, post-functionality and other useful properties³⁷. The post-modification of **HNTs** surface with **PDA** may modify the interfacial interactions between inorganic **HNTs** and inorganic **Bru-CPCs**.

Herein, aiming to improve the mechanical properties of bone repair materials, a novel **Bru-CPCs/1.5%HNTs** with **HNTs** was developed. The mechanical properties and biological activity of **Bru-CPCs/1.5%HNTs** scaffold were investigated. Considered of the interfacial interactions between **HNTs** and **Bru-CPCs** and the high adhesive property of **PDA**, **HNTs** surface was then coated by **PDA** layer. **Bru-CPCs/1.5%HNTs@PDA** scaffolds were constructed. The effect of **HNTs@PDA** on the mechanical properties and biological activity of those scaffolds were assessed and discussed in detail. All the results demonstrated that the adding **HNTs@PDA** can improve the compressive strength and bioactivity properties of **Bru-CPCs/1.5%HNTs@PDA** scaffolds for effective bone cell adhesion and growth, which may be widely used as bone repair materials in the further.

Results and discussion

Characterization of Bru-CPCs@HNTs. **Bru-CPCs** and modified **Bru-CPCs/HNTs** were first prepared, and the effect of **HNTs** content on the mechanical properties of **Bru-CPCs** were investigated, as shown in **Figure 1B** and **Figure S1**. The results revealed that the mechanical properties increased initially and then decreased with increasing the content of **HNTs**. The optimal mechanical performance was achieved with adding 1.5% **HNTs**, reaching 12.16 MPa. These findings indicate that **HNTs** can enhance the mechanical properties of the modified **Bru-CPCs/HNTs**. But the weak interfacial interaction between **HNTs** and **Bru-CPCs** constrains the potential enhancement of mechanical properties. Additionally, we tested the setting time, pH, and degradation performance, as depicted in **Figure S2**. The initial setting time for **Bru-CPCs** was found to be 10 minutes, and the final setting time was 21 minutes. For **Bru-CPCs/1.5%HNTs**, the initial setting time was 9 minutes, and the final setting time was 20 minutes. The addition of **HNTs** had a negligible effect on the setting time. After immersion in SBF solution for 12 hours, the pH of the samples was approximately 5.9. Since SBF was not a buffered system, the pH did not increase to 7.4 within 12 hours. The samples were then incubated for an additional 12 hours, and the pH reached 7.4. The pH values remained almost unchanged around 7.4 for all samples with further incubation. Regarding degradation performance, **Bru-CPCs/1.5%HNTs** exhibited a slightly slower degradation rate compared to **Bru-CPCs**. To further enhance the mechanical properties of **Bru-CPCs** and increase the interfacial interaction between **HNTs** and **Bru-CPCs**, we propose to modify **HNTs** by

introducing polydopamine to prepare **HNTs@PDA**. Subsequently, **HNTs@PDA** will be incorporated into **Bru-CPCs** to further improve their mechanical performance.

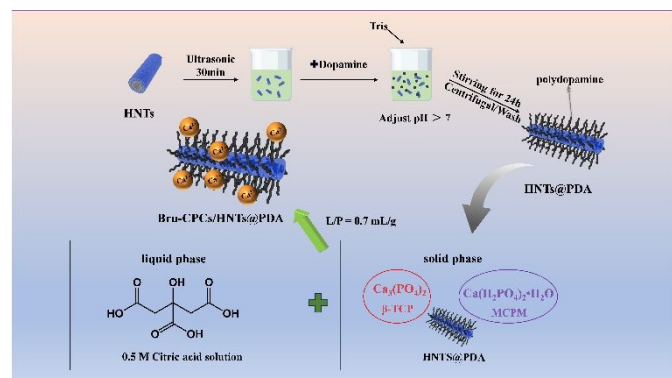
Preparation procedures and thermogravimetric analysis and morphology of HNTs@PDA. The preparation process was shown in **Scheme 1**. Briefly, **DA** and **HNTs** were stirred in an alkaline environment and a **PDA** coating was formed on the surface of **HNTs** by self-polymerization of **DA** to get **HNTs@PDA**. The morphological characters of **HNTs** and **HNTs@PDA** were revealed by TEM observations, which were shown in **Figure S3**. The unmodified **HNTs** exhibit a cylindrical morphology with a distinct, empty central lumen. The **HNTs** samples display an open-ended, hollow cylindrical structure with outer diameters ranging from 32-36 nm and inner diameters spanning 22-25 nm, respectively. The **HNTs** exhibit remarkably clear central channels, a testament to their double-layered nanotube architecture. Upon modification with dopamine, the **HNTs@PDA** display an enlarged outer diameter compared to the unmodified **HNTs**, indicative of a successful **PDA** coating on the exterior wall of the nanotubes³⁸. The **HNTs@PDA** exhibit a notable increase in wall thickness, and their outer surfaces appear roughened and coated with irregular materials, leading to an increase in the diameter of **HNTs** significantly³⁹. The thickness of **HNTs@PDA** layer (13-19 nm) is larger than that of **PDA** layer (8-10 nm), indicating the successful coating of **PDA** modification⁴⁰.

The corresponding elemental maps displayed in **Figure S4** shows that distribution of the constituent calcium element. The calcium mapping of the **Ca-HNTs@PDA** reveals an even distribution of the elemental signal along the entire length of the tube, indicating uniform enrichment of calcium ions. In contrast, the calcium mapping of the **Ca-HNTs** exhibits a random distribution pattern. The surface functionalization achieved through **PDA** coating enhances the accumulation of calcium ions within the material^{32, 41}. The strong affinity between calcium ions and the catechol groups present in **PDA** suggests a significant interfacial interaction, which can contribute to the enhanced interface forces between **HNTs@PDA** and **Bru-CPC**⁴².

We used thermogravimetric analysis to analyze the grafting rate of **PDA** on **HNTs** (**Figure 1A**). As shown in **Figure 1A**, the weight decreased upon increasing the temperature from ambient temperature to 800 °C. The weight loss in the temperature range of room temperature to 405 °C was attributed to the adsorbed water and the chemically grafted silane existing in **HNTs**. The weight loss in the temperature range of 405 °C to 535 °C was attributed to the dihydroxylation of structural Al-OH groups of **HNTs**^{43, 44}. The weight loss of **HNTs@PDA** increases after coating with **PDA**. After 800 °C, the remaining weight was 85.0% and 81.6% for **HNTs** and **HNTs@PDA**, respectively, which indicating that **PDA** has been successfully grafted onto **HNTs**. Moreover, an CCK-8 test was performed to investigate the cytocompatibility of the **HNTs** and **HNTs@PDA** by co-culturing MC3T3-E1 cells (**Figure S5**). The result showed that the number of cells in all groups increased with 24 hours, indicating **HNTs** and **HNTs@PDA** had good cell safety. After **PDA** functionalization, **HNTs** and **HNTs@PDA** were used as solid



additive to incorporated into Bru-CPCs to obtain Bru-CPCs/1.5% HNTs and Bru-CPCs/1.5% HNTs@PDA (Scheme 1).



Scheme 1. The preparation process of HNTs@PDA and scaffolds **Compressive strength, fracture morphology, porosity, and anti-washout property.**

Compressive strength, fracture morphology, and porosity. The scaffolds were molded to obtain cylindrical forms (Scheme 1). The compressive strength and anti-washout ability of CPCs, which were critical for the actual clinical use, were systematically investigated. The compressive strength of pure Bru-CPCs, Bru-CPCs/1.5% HNTs and Bru-CPCs/1.5% HNTs@PDA scaffolds were shown in Figure 1B and Figure S1. The compressive strength of Bru-CPCs was 8.87 MPa after 2 days of immersion, which was consistent with the literature^{44, 45}. As the content of HNTs increased to 1.5%, the value was increased to 12.16 MPa. The result showed that the addition of HNTs can improve the weak compressive strength of bone repair materials. A similar trend was observed for Bru-CPC/HNTs and Bru-CPC/HNTs@PDA shown in Figure S1. When adding 1.5 wt% HNTs@PDA, the compressive strength of Bru-CPCs/1.5% HNTs@PDA further increased to 18.14 MPa, which was about 2-fold higher than Bru-CPCs. The improving of compressive strength of bone repair material may be attributed to the strong affinity between catechol moieties of PDA and Ca²⁺ in Bru-CPCs. The fracture morphology of scaffolds was characterized by SEM (Figure 1C). The fracture morphology of Bru-CPCs was irregular plate-like or flaky brushite crystals with micron to nanometer sizes. HNTs can be acted as crystal nuclei. Hence, with adding HNTs, the plate-like crystallization of Bru-CPCs/1.5% HNTs was more regular. After introducing HNTs@PDA, the crystals of Bru-CPCs/1.5% HNTs@PDA are more regularly stacked and the grain size becomes smaller. Some interfaces become blurred. These results may be beneficial to improving the mechanical properties. Figure S6 exhibited the porosity of CPCs. The porosity of Bru-CPCs was about 42.22±0.75%. The porosities of Bru-CPCs/1.5% HNTs and Bru-CPCs/1.5% HNTs@PDA were 36.04±0.67% and 38.31±0.71%, respectively. The decrease in the porosity of CPCs may lead to an increase in compressive strength.

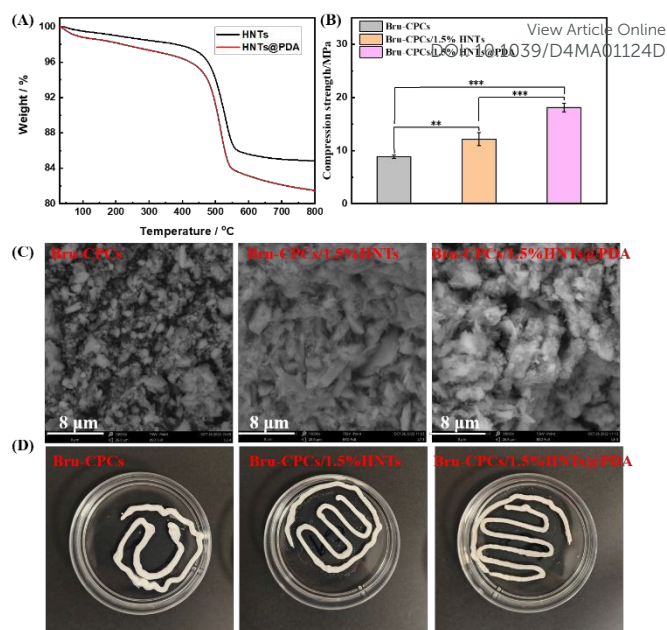


Figure 1. (A) TGA curves of HNTs and HNTs@PDA. (B) Compressive strength of CPCs scaffolds (incubated at 37 °C and 100% relative humidity for 2 days, **P < 0.01, ***P < 0.001). (C) Morphology of bone repair materials after mineralization. (D) Anti-washout property of CPCs scaffolds. Optical digital images of CPCs scaffolds after injected into PBS solution and shaken at a speed of 60 rpm at 60 min.

Anti-washout property. The anti-washout property of the CPCs was determined by the appearance integrity after CPCs was injected into the PBS solution as given in Figure 1D and Figure S7. CPCs had good continuous shapes when injected in PBS solution. After the 60 min of shaking cycles, Bru-CPCs/1.5% HNTs slightly disintegrated, while Bru-CPCs/1.5% HNTs@PDA showed more complete appearances. It might well be contributed by the chemical chelation of hydroxyl groups with Ca²⁺.^{46, 47} The post-modification of HNTs surface with PDA modify the interfacial interactions between inorganic HNTs and inorganic Bru-CPCs and enhanced the anti-washout property of Bru-CPCs/1.5% HNTs@PDA.

Adhesive property, CCK-8 analysis, and live/dead staining analysis.

Adhesive property. The adhesion and colonization of seed cell on the scaffolds are prerequisites for scaffold-dependent tissue engineering to promote bone regeneration⁴⁸. SEM images showed that the cells started to spread on the surface of Bru-CPCs, Bru-CPCs/1.5% HNTs and Bru-CPCs/1.5% HNTs@PDA. MC3T3-E1 cells on Bru-CPCs, Bru-CPCs/1.5% HNTs and Bru-CPCs/1.5% HNTs@PDA displayed by SEM observation exhibited flat with intact, well-defined morphology and extending filopodia (Figure 2A). This result indicated that all the scaffolds have good cytocompatibility.

CCK-8 analysis. CCK-8 analysis (Figure 2B) and live/dead staining (Figure 2C) were used to evaluate the proliferation of MC3T3-E1 cells on the scaffolds. As shown in Figure 2B, the relative cell proliferation rates were all higher than 70% (the cell survival rate of the control group is defined as 100%), indicating that cells proliferated well in each group. In the first day of cell culture, the relative cell proliferation rates in Bru-CPCs, Bru-CPCs/1.5% HNTs, and Bru-



CPCs/1.5%HNTs@PDA scaffolds were difference, about 101%, 108%, and 112%, respectively. On the 3rd days, the relative cell proliferation rates in **Bru-CPCs**, **Bru-CPCs/1.5%HNTs**, and **Bru-CPCs/1.5%HNTs@PDA** scaffolds were 124%, 128%, and 131%, respectively. The addition of **HNTs@PDA** increases the cell proliferation rate to a certain extent, which could be attributed to the comprehensive results of improved hydrophilicity, roughness, chemical composition, and morphology of the **HNTs@PDA** coating⁴⁹. **Live/dead staining analysis.** The results of live/dead staining analysis further verified the results of CCK-8 analysis. As shown in **Figure 2C**, the living MC3T3-E1 cells were stained green and displayed a normal shape. Compared with the control group and the pure **Bru-CPCs** scaffold, with the addition of **HNTs** and **HNTs@PDA**, the live cells (green fluorescence) density in the **Bru-CPCs/1.5%HNTs** scaffold and the **Bru-CPCs/1.5%HNTs@PDA** scaffold increased and dew dead cells (red fluorescence) were observed. All the results demonstrated that **Bru-CPCs/1.5%HNTs@PDA** scaffold promoted cell adhesion and proliferation and exhibited no adverse effects on cell viability and morphology.

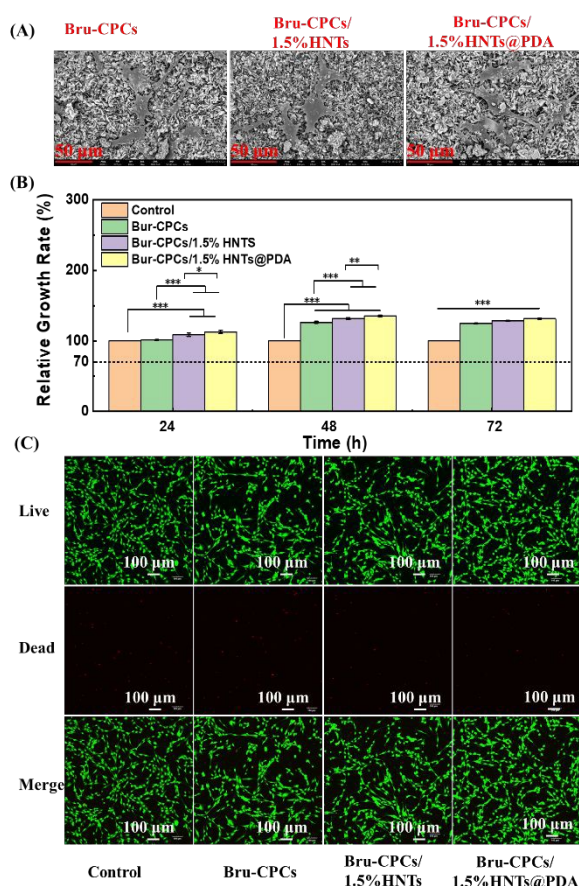


Figure 2. (A) SEM images of scaffolds co-cultured with cells for 24 h. (B) Cell viability of scaffolds, CCK-8 test (* $P < 0.05$, ** $P < 0.01$, *** $P < 0.001$). (C) Live/dead staining images of bone repair materials after co-culturing with cells for 24 hours.

ALP staining, ALP activity, and In vitro osteogenesis properties.

ALP staining and ALP activity. Alkaline phosphatase (ALP) was an early osteogenic marker, which can reflect the differentiation trend and mineralization ability of osteoblasts⁵⁰. The osteogenic induction

of scaffolds was determined by ALP staining after 7 days of co-cultivation. The ALP expression of all scaffolds and the control group were positive (**Figure 3A**), indicating that all the scaffolds have the potential to promote the early osteogenic differentiation. To more intuitively understand the differences in ALP activity of bone repair materials, ALP activity was detected (**Figure 3B**). Compared with the control group, the ALP activities of **Bru-CPCs**, **Bru-CPCs/1.5%HNTs**, and **Bru-CPCs/1.5%HNTs@PDA** are all significantly increased.

In vitro osteogenesis properties. To elucidate the moderating effect of **HNTs** and **HNTs@PDA** on osteogenic genes in MC3T3-E1 cells, we performed RT-qPCR for 5 related osteogenesis genes (Col-I, IBSP, OCN, OPN, and Runx2). **Figure 3C** shown the expressions of Col-I, IBSP, OCN, OPN, and Runx2 of MC3T3-E1 after co-culturing with **Bru-CPCs**, **Bru-CPCs/1.5%HNTs**, and **Bru-CPCs/1.5%HNTs@PDA**. After culturing for 7 days, the different scaffolds upregulated the expression of 5 related osteogenesis genes to varying degrees. The cells in the group treated with **Bru-CPCs/1.5%HNTs** exhibited a higher expression of Col-I, IBSP, OCN, OPN and Runx2 than the control group and **Bru-CPCs** group in 7 days. While, the expression levels of Col-I, IBSP, OCN and OPN in the **Bru-CPCs/1.5%HNTs@PDA** group had significant difference with the other groups. Based on the higher expression levels of the four genes, it could be seen that addition **HNTs@PDA** into bone repair materials did not impair the osteoconductive function. **Bru-CPCs/1.5%HNTs@PDA** is conducive to the osteogenic differentiation and promote bone repair.

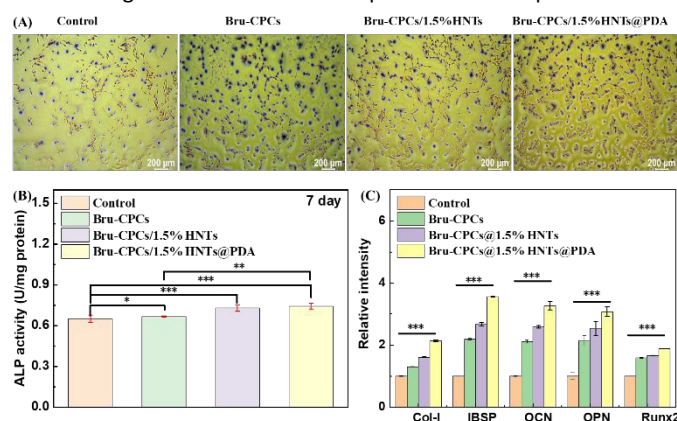


Figure 3. (A) ALP staining, (B) ALP activity and (C) Osteogenesis-related gene expression test of scaffolds (* $P < 0.05$, ** $P < 0.01$, *** $P < 0.001$).

Conclusions

In this study, **HNTs** was incorporated into the **Bru-CPCs** as an additive to enhance the mechanical properties and osteogenic bioactivity of CPCs. The result indicated that the addition of **HNTs** led to an increase in the compressive strength of the CPCs. Additionally, the proliferation and in vitro osteogenic differentiation of MC3T3-E1 cells were also improved. The strong affinity between calcium ions and the catechol groups in **PDA** suggests significant interfacial interaction, which may contribute to the enhanced interface forces between **HNTs@PDA** and **Bru-CPCs**. The interfacial interactions between **HNTs** and **Bru-CPCs** are critical in further augmenting the compressive strength of the CPCs. Subsequently, **HNTs** surface was coated by **PDA** layer and **Bru-CPCs/1.5%HNTs@PDA** was fabricated.



The **Bru-CPCs/1.5%HNTs@PDA** scaffold exhibited superior compressive strength, cell proliferation, and osteogenic differentiation properties compared to both the **Bru-CPCs** and the **Bru-CPCs/1.5%HNTs** scaffolds. Based on these results, the newly designed **Bru-CPCs/1.5%HNTs@PDA** emerges as promising candidate for bone-tissue repair applications. This work provides an efficient and universal strategy to design and construction of high-performance personalized materials for bone-tissue regeneration. Further research will be focus on in vivo studies and clinical evaluations, which are essential to ascertain the stability and regenerative potential of the fabricated scaffolds in the context of bone-tissue regeneration.

Conflicts of interest

There are no conflicts to declare.

Acknowledgements

This study was supported by the National Natural Science Foundation of China (No. 22202055), the Natural Science Foundation of Hebei Province, China (No. C2022201038, H2022201017), the Foundation of Hebei Education Department (No. BJK2023004), Foundation of President of Hebei University (No. XZJJ202005), Medical Science Foundation of Hebei University (No. 2021B03), and the "Advanced Talents Incubation Program of the Hebei University".

References

- Huang, A. C. Santos, Q. Tan, H. Bai, X. Hu, N. Mamidi and Z. Wu, *J. Nanobiotechnol.*, 2022, **20**, 522.
- N. Z. Laird, T. M. Aciri, K. Tingle and A. K. Salem, *Adv. Drug Delivery Rev.*, 2021, **174**, 613-627.
- L. Sun, H. Niu, Y. Wu, S. Dong, X. Li, B. Y. S. Kim, C. Liu, Y. Ma, W. Jiang and Y. Yuan, *Bioact. Mater.*, 2024, **35**, 208-227.
- X. He, Y. Li, D. Zou, H. Zu, W. Li and Y. Zheng, *Bioact. Mater.*, 2023, **456**-478.
- L. Chen, J. Yang, Z. Cai, Y. Huang, P. Xiao, J. Wang, F. Wang, W. Huang, W. Cui and N. Hu, *Adv. Funct. Mater.*, 2024, **34**, 2314079.
- J. D. Schwartzman, M. McCall, Y. Ghattas, A. S. Pugazhendhi, F. Wei, C. Ngo, J. Ruiz, S. Seal and M. J. Coathup, *Biomaterials*, 2024, **311**, 122683.
- M. Li, H. Wu, K. Gao, Y. Wang, J. Hu, Z. Guo, R. Hu, M. Zhang, X. Pang, M. Guo, Y. Liu, L. Zhao, W. He, S. Ding, W. Li and W. Cheng, *Adv. Healthcare Mater.*, 2024, **13**, 2402916.
- A. Vezenkova and J. Locs, *Bioact. Mater.*, 2022, **17**, 109-124.
- H. H. K. Xu, P. Wang, L. Wang, C. Bao, Q. Chen, M. D. Weir, L. C. Chow, L. Zhao, X. Zhou and M. A. Reynolds, *Bone Res.*, 2017, **5**, 17056.
- C. Cui, D. Liu, X. Xie, L. Wang, M. J. Lukic, X. Qiu, W. Chen, J. Shi, Y. Hong, B. Li, Z. Liu and S. Chen, *Composites, Part B*, 2024, **287**, 111812.
- W. Zhi, X. Wang, D. Sun, T. Chen, B. Yuan, X. Li, X. Chen, J. Wang, Z. Xie, X. Zhu, K. Zhang and X. Zhang, *Bioact. Mater.*, 2022, **11**, 240-253.
- Y. Feng, D. Wu, J. Knaus, S. Keßler, B. Ni, Z. Chen, J. Avaro, R. Xiong, H. Cölfen and Z. Wang, *Adv. Healthcare Mater.*, 2023, **12**, 2203411.
- K. Hurle, J. M. Oliveira, R. L. Reis, S. Pina and F. Goetz-Neunhoffer, *Acta Biomater.*, 2021, **123**, 51-71.
- W. Gao, H. Wang, R. Liu, X. Ba, K. Deng and F. Liu, *ACS Biomater. Sci. Eng.*, 2024, **10**, 2062-2067.
- L. Ding, H. Wang, J. Li, D. Liu, J. Bai, Z. Yuan, J. Yang, L. Bian, X. Zhao, B. Li and S. Chen, *Biomater. Sci.*, 2023, **11**, 96-107.
- G. Tripathi, M. Park, M. Hossain, S. B. Im and B. T. Lee, *Int. J. Biol. Macromol.*, 2022, **221**, 1536-1544.
- N. Ribeiro, M. Reis, L. Figueiredo, A. Pimenta, L. F. Santos, A. C. Branco, A. P. Alves de Matos, M. Salema-Oom, A. Almeida, M. F. C. Pereira, R. Colaço and A. P. Serro, *Ceram. Int.*, 2022, **48**, 33361-33372.
- P. A. Krokhicheva, M. A. Goldberg, A. S. Fomin, D. R. Khayrutdinova, O. S. Antonova, A. S. Baikin, A. A. Konovalov, A. V. Leonov, I. V. Mikheev, E. M. Merzlyak, V. A. Kirsanova, I. K. Sviridova, N. S. Sergeeva, S. M. Barinov and V. S. Komlev, *Ceram. Int.*, 2023, **49**, 19249-19264.
- W. Liu, J. Zhang, P. Weiss, F. Tancret and J.-M. Bouler, *Acta Biomater.*, 2013, **9**, 5740-5750.
- Y. Wan, H. Ma, Z. Ma, L. Tan and L. Miao, *ACS Biomater. Sci. Eng.*, 2023, **9**, 6084-6093.
- G. H. Lee, P. Makkar, K. Paul and B. Lee, *Mater. Sci. Eng. C.*, 2017, **77**, 713-724.
- M. Roozbahani and M. Kharaziha, *Biomed. Mater.*, 2019, **14**, 055008.
- F. Kazemi-Aghdam, V. Jahed, M. Dehghan-Niri, F. Ganji and E. Vasheghani-Farahani, *Carbohydr. Polym.*, 2021, **269**, 118311.
- L. Tong, Q. Liu, L. Xiong, P. Wang, M. Zhao, X. Li, J. Liang, Y. Fan, X. Zhang and Y. Sun, *Sci. China Mater.*, 2024, **67**, 2067-2079.
- F. Doustdar, A. Olad and M. Ghorbani, *Carbohydr. Polym.*, 2022, **282**, 119127.
- J. Liao, H. Wang, N. Liu and H. Yang, *Adv. Colloid Interface Sci.*, 2023, **311**, 102812.
- E. Torres, V. Fombuena, A. Vallés-Lluch and T. Ellingham, *Mater. Sci. Eng. C.*, 2017, **75**, 418-424.
- J. Varshosaz, Z. S. Sajadi-Javan, M. Kouhi and M. Mirian, *Int. J. Biol. Macromol.*, 2021, **192**, 869-882.
- J. Zheng, F. Wu, H. Li and M. Liu, *Mater. Sci. Eng. C.*, 2019, **105**, 110072.
- K. Huang, Q. Ou, Y. Xie, X. Chen, Y. Fang, C. Huang, Y. Wang, Z. Gu and J. Wu, *ACS Biomater. Sci. Eng.*, 2019, **5**, 4037-4047.
- D. M. Reffitt, N. Ogston, R. Jugdaohsingh, H. F. J. Cheung, B. A. J. Evans, R. P. H. Thompson, J. J. Powell and G. N. Hampson, *Bone*, 2003, **32**, 127-135.
- R. Wang, X. Zha, J. Chen, R. Fu, Y. Fu, J. Xiang, W. Yang and L. Zhao, *Adv. Healthcare Mater.*, 2024, **13**, 2304232.
- M. Mousa, N. D. Evans, R. O. C. Oreffo and J. I. Dawson, *Biomaterials*, 2018, **159**, 204-214.
- L. Ji, W. Qiao, Y. Zhang, H. Wu, S. Miao, Z. Cheng, Q. Gong, J. Liang and A. Zhu, *Mater. Sci. Eng. C.*, 2017, **78**, 362-369.
- Y. Zhou, X. Gao, M. Zhao, L. Li and M. Liu, *Compos. Sci. Technol.*, 2024, **250**, 110537.
- Q. Ou, K. Huang, C. Fu, C. Huang, Y. Fang, Z. Gu, J. Wu and Y. Wang, *Chem. Eng. J.*, 2020, **382**, 123019.
- J. Wang, Y. Cui, B. Zhang, S. Sun, H. Xu, M. Yao, D. Wu and Y. Wang, *Mater. Des.*, 2024, **238**, 112655.



ARTICLE

Journal Name

38. S. Choi, S. Chaudhari, H. Shin, K. Cho, D. Lee, M. Shon, S. Nam and Y. Park, *J. Ind. Eng. Chem.*, 2022, **105**, 158-170.
39. D. Gnanasekaran, A. Shanavas, W. W. Focke and R. Sadiku, *RSC Adv.*, 2015, **5**, 11272-11283.
40. C. Chao, J. Liu, J. Wang, Y. Zhang, B. Zhang, Y. Zhang, X. Xiang and R. Chen, *ACS Appl. Mater. Interfaces*, 2013, **5**, 10559-10564.
41. S. Kim and C. B. Park, *Biomaterials*, 2010, **31**, 6628-6634.
42. N. Holten-Andersen, T. E. Mates, M. S. Toprak, G. D. Stucky, F. W. Zok and J. H. Waite, *Langmuir*, 2009, **25**, 3323-3326.
43. Z. Wang, H. Wang, J. Liu and Y. Zhang, *Desalination*, 2014, **344**, 313-320.
44. Y. Zhang, R. Meng, J. Zhou, X. Liu and W. Guo, *Colloids Surf., A*, 2022, **648**, 129378.
45. H.-J. Lee, B. Kim, A. R. Padalhin and B.-T. Lee, *Mater. Sci. Eng. C*, 2019, **94**, 385-392.
46. H. Shi, X. Ye, J. Zhang and J. Ye, *ACS Biomater. Sci. Eng.*, 2019, **5**, 262-271.
47. L. Ding, H. Wang, W. Zhang, J. Li, D. Liu, F. Han, S. Chen and B. Li, *J. Mater. Chem. B*, 2021, **9**, 6802-6810.
48. B. G. Sengers, M. Taylor, C. P. Please and R. O. C. Oreffo, *Biomaterials*, 2007, **28**, 1926-1940.
49. Y. Yu, X. Li, J. Li, D. Li, Q. Wang and W. Teng, *Mater. Sci. Eng. C*, 2021, **131**, 112473.
50. Y. Wang, C. J. E. Davey, K. van der Maas, R.-J. van Putten, A. Tietema, J. R. Parsons and G.-J. M. Gruter, *Sci. Total Environ.*, 2022, **815**, 152781.

View Article Online
DOI: 10.1039/D4MA01124D



Due to the confidentiality of data, the data including raw files used or analyzed during the current study are available from the corresponding authors on reasonable request.

[View Article Online](#)

DOI: 10.1039/D4MA01124D

